ISSN 1027-4510, Journal of Surface Investigation: X-ray, Synchrotron and Neutron Techniques, 2023, Vol. 17, Suppl. 1, pp. S35–S42. © Pleiades Publishing, Ltd., 2023.

Ceramic Coatings Based on Chromium and Aluminum Nitrides Obtained by Vacuum-Arc Plasma-Assisted Evaporation

A. A. Leonov[a, *], Yu. A. Denisova[a], V. V. Denisov[a, **], M. S. Syrtanov[b], and A. N. Shmakov[c]

[a] *Institute of High Current Electronics, Siberian Branch, Russian Academy of Sciences, Tomsk, 634055 Russia*

[b] *National Research Tomsk Polytechnic University, Tomsk, 634050 Russia*

[c] *Budker Institute of Nuclear Physics, Siberian Branch, Russian Academy of Sciences, Novosibirsk, 630090 Russia*

**e-mail: laa-91@yandex.ru*

***e-mail: volodyadenisov@yandex.ru*

Received June 26, 2023; revised August 14, 2023; accepted August 14, 2023

Abstract—The results of studying multilayer CrN/AlN coatings obtained by vacuum-arc plasma-assisted evaporation at different speeds of rotation of the sample holder, as a result of which the thickness of individual CrN and AlN layers is assumed to be changed, are presented. The coatings are deposited onto a substrate made of VK8 hard alloy (WC + 8% of Co). The thickness of all multilayer CrN/AlN coatings is about 3 μm. Using energy-dispersive X-ray spectroscopy, it is shown that the CrN/AlN coatings under study have almost the same elemental composition. According to the results of X-ray phase analysis, it is found that CrN/AlN coatings have a two-phase structure consisting of CrN and AlN phases with a face-centered cubic (fcc) lattice. Nanoindentation revealed that the nanohardness values of CrN/AlN coatings vary from 28 to 33 GPa within the confidence interval, i.e., practically independent of the evaporation modes. The best tribotechnical characteristics are exhibited by CrN/AlN coatings obtained at a rotation speed of 5 rpm; it is likely that under this deposition condition, the optimal thickness of the CrN and AlN layers is achieved. By X-ray phase analysis using synchrotron radiation, it is found that chromium and aluminum nitrides retain thermal stability during heating to a temperature of ~1110–1115°C in air, and at least to a temperature of 1300°C in vacuum.

Keywords: nitride coatings, nanohardness, X-ray diffraction analysis, tribotechnical properties, friction coefficient, synchrotron radiation, thermal resistance

DOI: 10.1134/S1027451023070303

INTRODUCTION

At the end of the 20th century, the TiN, TiCN, and CrN coatings were widely used in the cutting-tool industry, but these coatings do not maintain their properties at high temperatures, which are encountered during processing under extreme cutting conditions [1–5]. The introduction of Al to the structure of CrN and TiN coatings allows one to solve this problem and improve the heat resistance and wear resistance of the composite coating [6]. The formation of a thin layer of Al_2O_3 on the surface of the coating prevents the further diffusion of oxygen into the coating, which increases the operating properties of the coated tool [7–11]. The deposition of multilayer coatings with a periodic nanocomposite structure is another approach that makes it possible to increase the physical, mechanical, tribological, and thermal properties of coatings compared to single-layer coatings of the same composition [12].

To achieve improved properties of multilayer coatings, alternating layers must have precise interfaces and optimized periodicity [13, 14]. As a rule, such coatings have increased hardness on account of the fact that numerous alternating nanolayers limit the propagation of dislocations [15] and the layers have different microstresses of the crystal lattices [16]; this is also explained by the Köhler effect (difference between layers in the elastic modulus) [17] and the Hall–Petch effect [18]. In addition, multilayer coatings with a periodic nanocomposite structure were found to have increased adhesion and improved impact strength [19], as well as improved corrosion resistance [20] and wear resistance [21]. Moreover, multilayer coatings were found to have improved thermal stability and oxidation resistance due to multiple interfaces acting as barriers to the internal and external diffusion of ions/atoms [22].

In [23], multilayer CrN/AlN coatings with a layer period (λ) of 4.8 nm had maximum hardness and resistance to plastic deformation (H^3/E^2), which are equal to 37 and 0.48 GPa, respectively. These values are 1.6 and 2.5 times higher than those of a single-layer CrN coating (23.5 and 0.17 GPa), respectively. Multilayer CrN/AlN coatings [24] with an optimized layer

period of 4.1 nm (CrN-layer thickness of 1.5 nm, AlN-layer thickness of 2.5 nm) had a maximum nanohardness of 42 GPa and the best tribotechnical characteristics (friction coefficient of 0.35 and wear parameter of 7×10^{-7} mm^3 N^{-1} m^{-1}) compared to a homogeneous $Cr_{0.4}Al_{0.6}N$ coating, which had a nanohardness of about 34 GPa, a friction coefficient of 0.42, and a wear parameter of 3.2×10^{-6} mm^3 N^{-1} m^{-1}.

The thicknesses of individual CrN and AlN nanolayers are varied by changing the target power [12, 25, 26], the rotation speed of the substrate holder [25], and the switching time of alternating shutters [27]. From published data it was revealed that there are very few studies on the production of multilayer CrN/AlN coatings using the vacuum-arc method [28, 29]. However, the vacuum-arc method of coating deposition has significant advantages such as a high ionization rate, good adhesion of coatings to the substrate, and a dense coating structure.

In [28], CrN/AlN and CrN/AlN/Al_2O_3 coatings deposited using the pulsed vacuum-arc method were studied. The hardness values of the CrN/AlN and CrN/AlN/Al_2O_3 coatings under study were 31.5 ± 1.9 GPa and 12.1 ± 1.7 GPa, respectively. The lower hardness of the CrN/AlN/Al_2O_3 coating is due to the top finishing layer of Al_2O_3, but this layer increased chemical inertness and thermal stability.

In [29], the AlCrN coating was deposited by the vacuum-arc method using separate cathodes made of aluminum and chromium. Both single-layer and multilayer coatings with different aluminum contents were deposited. It was shown that the rate of oxidation decreases with increasing aluminum content. The results of the above work showed that CrN/(Cr:Al)N multilayer coatings have both improved physical and mechanical properties and improved oxidation resistance.

In [30], the phase composition of CrN and CrAlN coatings was studied using high-temperature synchrotron radiation. For CrN coatings, the main phase in the entire temperature range (25, 200, and 500°C) was the CrN phase, and at temperatures above 600°C, the Cr_2N phase was formed. For CrAlN coatings, the main phase over the entire temperature range was the CrN phase. The cubic phase of *c*-AlN was observed up to 500°C. Starting from 600°C the *c*-AlN phase disappeared. Due to the similarity of the crystal lattices of the CrN and *c*-AlN phases, it is possible that they form a solid solution, since a shift of peaks in the diffraction pattern of CrN was observed with increasing temperature. Above 600°C, a significant amount of the Cr phase and a small amount of the AlO_2 phase appeared.

The aim of this study is to investigate the structure, phase composition, physical, mechanical, and tribological properties, and thermal resistance of CrN/AlN coatings obtained on VK8 hard alloy using vacuum-arc plasma-assisted sputtering when changing the rotation speed of the samples.

EXPERIMENTAL

Coating deposition was carried out using the vacuum-arc plasma-assisted method on an modernized NNV6.6-I1 setup equipped with two electric-arc evaporators with a cathode diameter of 80 mm and an additional PINK gas-plasma source [31, 32]. The high-vacuum pumping system of the setup was based on the TMN-1000 turbomolecular pump. The setup had a planetary rotation system for the sample holder and an injection system for two gases (Ar and N_2). Electric-arc sources with chromium (purity 99.5%) and aluminum (purity 99.8%) cathodes were located on the side walls of the working chamber. The PINK gas-plasma source was mounted on the door of the vacuum chamber. The inner walls of the vacuum chamber made of stainless steel served as an anode for the sources of metal and gas plasma. The PINK gas-plasma source was used for cleaning, heating, and additional ionization of both the gas component of the plasma, which provides an assistive effect on the growing layers of the coating, and the metal component of the plasma.

The samples with a diameter of 10 mm and a thickness of 7 mm for coating were made of VK8 hard alloy (WC + 8% of Co). The samples were pre-polished and, before loading into a vacuum chamber, cleaned in an ultrasonic bath in gasoline and then in acetone. During deposition, the holder with the samples was rotated around the central axis of the chamber at a distance of 200 mm from it, as well as around its own axis. Before the experiment began, the vacuum chamber was evacuated with a turbomolecular pump to a maximum pressure of 2×10^{-2} Pa. By supplying the working argon gas through the PINK plasma source, the working pressure was set at 0.3 Pa. When a gas discharge was ignited and a bias voltage of (–600) V was applied to the holder with the samples, the samples were heated to a temperature of about 400°C. After cleaning the surface of the samples by ion bombardment and its chemical activation, the simultaneous ignition of discharges in the electric-arc evaporators was initiated and sputtering of the coating was carried out. The current of the gas-plasma source did not change in all sputtering modes and was about 90 A. The optimal current values for electric-arc evaporators were selected in a series of preliminary studies and amounted to 80 A (Cr cathode) and 30 A (Al cathode). When sputtering nitrides, high-purity nitrogen with a small, up to 10%, addition of argon was injected. The sputtering time in all modes was 120 minutes. The negative bias voltage was 150 V for all deposition modes. When evaporating the coatings, the table rotation speed was varied to 0.5, 3.5, 5, 8, and 12 rpm in order to change the thickness of the deposited layers. The table rotation speed values were used to further

designate the CrN/AlN coating samples. The thickness of the coatings was about 3 μm.

The surface structure of the coated samples was studied using scanning electron microscopy (SEM-515 Philips). The elemental composition of the coatings was studied using a Genesis energy-dispersive X-ray microanalyzer built into a Philips SEM-515 scanning electron microscope. The phase composition of the coatings was determined by X-ray diffraction analysis using a Shimadzu XRD-7000S diffractometer with CuK_α radiation. The phase composition was analyzed using the Crystallographica Search-Match program and PDF 4+ databases, as well as the Powder Cell 2.4 full-profile analysis program [33–35]. Nanoindentation of the coatings under study was carried out using a NANO Hardness Tester NHT-S-AX-000X. Using a Berkovich indenter, the load applied to the sample surface was increased from 0 to 20 mN at a loading rate of 1.5 μm/min and then decreased at the same rate to 0 at a frequency of 10 Hz. The nanoindentation data were analyzed using the Oliver–Pharr method. Tribotechnical tests of the coatings were carried out on a Tribotechnic tribometer under dry-friction conditions when the sample moved relative to the counterbody. An Al_2O_3 ball with a diameter of 6 mm was used as the counterbody. The sample movement speed during testing was 25 mm/s. The load on the counterbody was 5 N, the track radius was 3 mm, and the friction path was 300 m. During testing, the current values of the friction coefficient were recorded. Tests comply with ISO 7148, ASTM G99-95a, and ASTM G 133-95 international standards. The surface roughness of the initial VK8 sample and samples with CrN/AlN coatings was determined using a contact profilometer. The surface roughness of the VK8 samples was about 53 nm before deposition. The resistance to high-temperature oxidation and stability of the structural-phase state of CrN/AlN ceramic coatings were studied in the temperature range from 30 to 1300°C by X-ray phase analysis using synchrotron radiation. The source of synchrotron radiation was the VEPP-3 electron storage ring (Budker Institute of Nuclear Physics, Siberian Branch, Russian Academy of Sciences, Novosibirsk). The study was carried out using an HTK-2000 high-temperature X-ray camera, an OD-3M-350 position-sensitive single-axis detector, and software: the program for processing the measurement results Fityk v.1.3.1. The studies were carried out under the following experimental conditions: operating radiation wavelength of $\lambda = 0.172$ nm, diffraction-angle range 2θ from 28° to 59°, and sample heating rate of 10°C/min. The measurement results were processed using the program for processing measurement results Fityk v.1.3.1.

RESULTS AND DISCUSSION

Figure 1 shows a SEM image of the surface of the sample with a CrN/AlN coating, from which the elemental composition was measured. It is clear from the SEM image that there are microdroplets on the surface of the coating, the diameter of which can reach more than 20 μm. Predominantly, the droplets consist of aluminum. In addition, it can be noted that the size of the droplets and their number do not depend on the sputtering modes. Microdroplets are formed as a result of the evaporation of cathode material in cathode spots due to the high temperature of the arc discharge and are deposited onto the substrate.

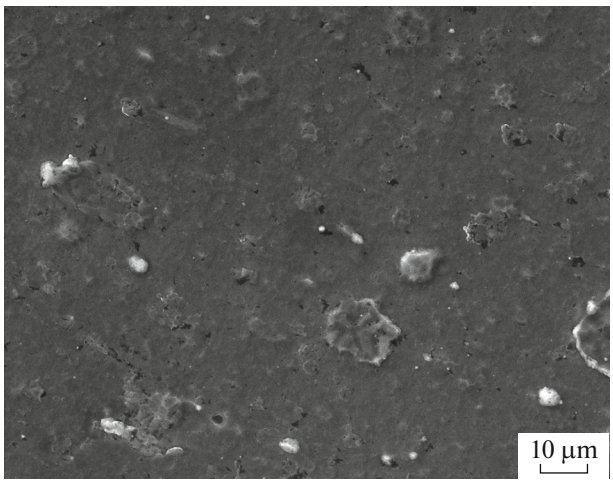

Fig 1. SEM image of the surface of a sample with a CrN/AlN coating obtained at a rotation speed of 5 rpm.

Using energy-dispersive X-ray spectroscopy, it was discovered that changes in the rotation speed of the table with the sample holder have virtually no effect on the elemental composition of the coatings. All coatings have an almost identical Cr/Al ratio, which is expected since the power supplied to the Cr and Al cathodes was kept constant.

Figure 2 shows the X-ray diffraction patterns obtained from CrN/AlN coatings. The coatings have a two-phase structure consisting of CrN and AlN phases with a face-centered cubic lattice. Aluminum nitride is stable in a hexagonal structure under normal conditions. One way to stabilize the cubic structure of aluminum nitride is to alloy it with titanium or chromium. With this sputtering method, the simultaneous deposition of aluminum and chromium and partial mixing occur. As a result, the cubic structure of aluminum nitride is stabilized in the coating. All diffraction patterns also contain reflections of pure aluminum.

Figure 3 shows the dependence of the content of all phases for samples deposited at different table rotation speeds, from which it can be seen that with increasing table rotation speed from 3.5 to 12 rpm, there is a gradual increase in the amount of aluminum nitride AlN from 16.5 to 41.4 vol %. In addition, with increasing speed, the volume fraction of aluminum in the coatings decreases.

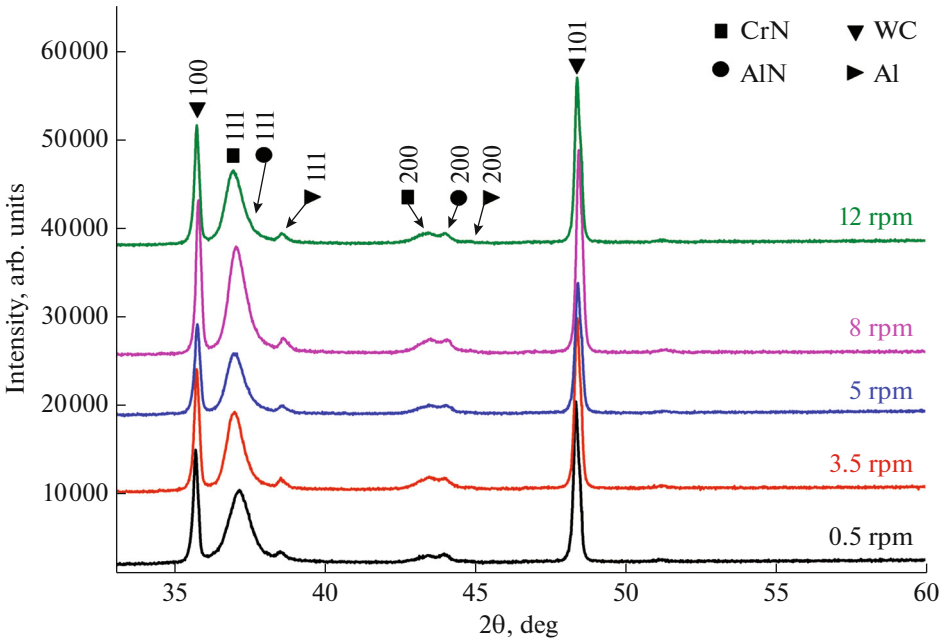

Fig. 2. X-ray diffraction patterns of the studied CrN/AlN coatings.

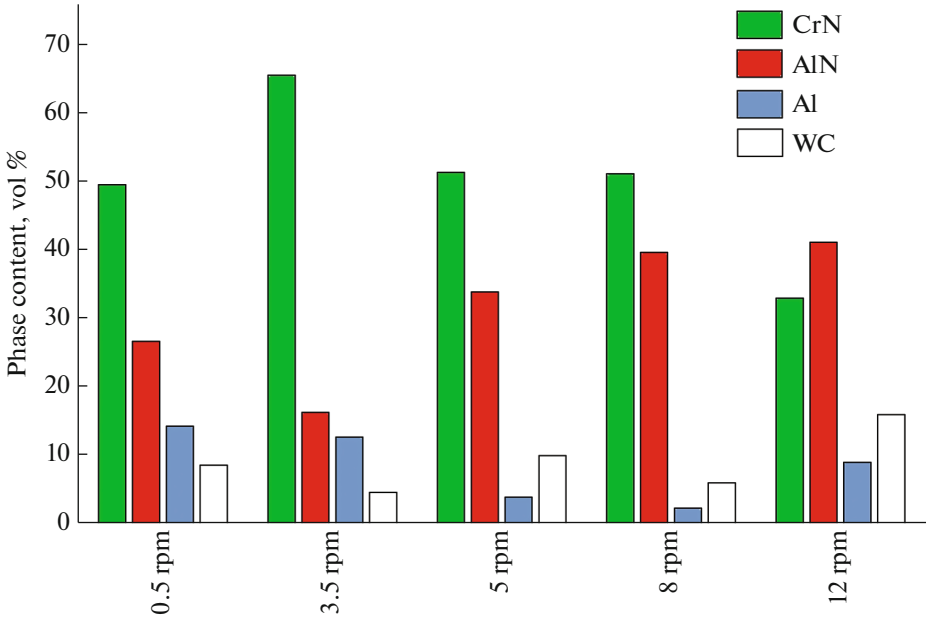

Fig. 3. Volume fraction of phases in the coatings under study.

The size of coherent-scattering regions (CSR) in the coatings varies from 2 to 44 nm for CrN and from 16 to 38 nm for AlN (Table 1). From Table 1, it can be seen that during sputtering with increasing rotation speed, i.e., with decreasing layer thickness, microstresses in the AlN layers tend to decrease, and in the CrN layers they tend to increase.

The physical and mechanical properties of the coatings were studied by nanoindentation. Figure 4 shows the typical loading curves during nanoindentation. The load was selected in such a way that the indenter penetration depth was less than 1/10 of the coating thickness (Buckle's rule, 1959) to exclude the influence of the substrate [37–40]. Figure 4 shows that the obtained curves are similar to each other and the maximum indentation depth ranges from 200 to 213 nm, which is less than 1/10 of the thickness of the coatings under study, since the average thickness was

Table 1. Parameters of the crystal structure of the studied CrN/AlN coatings

Sample	Lattice parameter, *a*		CSR size, nm		Microstress	
	CrN	AlN	CrN	AlN	CrN	AlN
0.5 rpm	4.1832	4.1030	30	38	0.004316	0.002445
3.5 rpm	4.2002	4.1130	–	16	–	0.002878
5 rpm	4.1840	4.094	29	28	0.006284	0.001250
8 rpm	4.1794	4.0924	44	23	0.007363	0.001715
12 rpm	4.1571	4.1123	33	29	0.001113	0.002147

about 3 μm. On the basis of data processing by the Oliver—Pharr method using specialized software, the values of the nanohardness (H) and elastic modulus (E) were obtained (Table 2). From Table 2, it can be seen that the H values of the coatings vary from 28 to 33 GPa within the confidence interval, i.e., they barely depend on the deposition modes. The maximum values of E were obtained for coating samples 0.5 rpm and 12 rpm and are 411 and 431 GPa, respectively.

In [41], the CrN/AlN coatings with a layer period Λ from 2.0 to 4.7 nm had a nanohardness above 30 GPa, where the AlN layers had a face-centered cubic lattice of the NaCl type. However, when the layer period Λ increased to more than 6.0 nm (up to 22.5 nm), where the AlN layers had a wurtzite-type structure, a significant decrease in hardness was observed up to 23–25 GPa. In our case, the nanohardness varies from 28 to 33 GPa, the coatings under study have only the fcc AlN structure, and therefore, it can be assumed that the resulting CrN/AlN coatings have a layer period Λ of less than 6 nm. The H/E ratio is often used as a measure of assessing the resistance of the coating to elastic deformation, while it is assumed that H/E greater than or equal to 0.1 indicates its high quality. From the data obtained, it follows (Table 2) that the CrN/AlN coatings under study can be considered of insufficient quality.

Figure 5 shows the values of the wear parameter and friction coefficient of the CrN/AlN coatings under study. The lowest friction-coefficient values of 0.462 and wear-parameter values in the low range of 10^{-7} mm^3/N m were observed in CrN/AlN coatings obtained at a rotation speed of 5 rpm. Probably, this improvement in tribotechnical properties with an increase in rotation speed from 0.5 to 5 rpm is related to a decrease in the thickness of each CrN and AlN layer. The CrN/AlN coatings obtained at higher rotation speeds (8 and 12 rpm) demonstrate higher friction-coefficient values in the range from 0.503 to 0.523 and have greater wear, the values of which are approximately two times higher compared to coatings obtained at 5 rpm. The obtained values of the wear

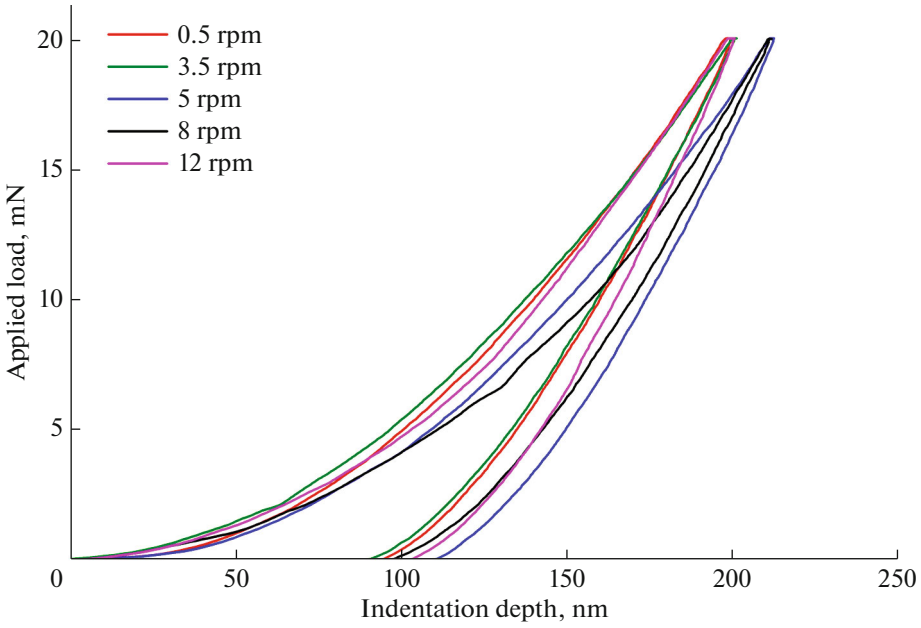

Fig. 4. Loading–unloading curves obtained by nanoindentation of the studied CrN/AlN coatings.

Table 2. Results of nanoindentation

Sample	*H*, GPa	*E*, GPa	*H*/*E*
0.5 rpm	33 ± 4	411 ± 35	0.08
3.5 rpm	28 ± 5	355 ± 29	0.08
5 rpm	30 ± 4	399 ± 25	0.08
8 rpm	33 ± 4	382 ± 57	0.09
12 rpm	30 ± 5	431 ± 41	0.07

parameter and friction coefficient of CrN/AlN coatings at increased rotation speeds (8 and 12 rpm) are similar to the values characteristic of homogeneous $Cr_{1-x}Al_xN$ coatings with different Al contents, as reported in [24, 42], which suggests that at such rotation speeds, layers of CrN and AlN that are too thin are formed, and perhaps a blurred interface is formed between the layers. Typically, the wear parameter has a similar trend compared to the change in the friction coefficient in CrN/AlN coatings (Fig. 5) [42]. In general, a higher coefficient of friction results in a higher wear rate.

Figure 6 shows complete sets of diffraction patterns of CrN/AlN:12 rpm coatings during heating from room temperature to 1300°C in air (Fig. 6a) and in a vacuum chamber with a residual pressure of $P = 5 \times 10^{-3}$ mbar (Fig. 6b) obtained by X-ray phase analysis using synchrotron radiation. The CrN/AlN coating

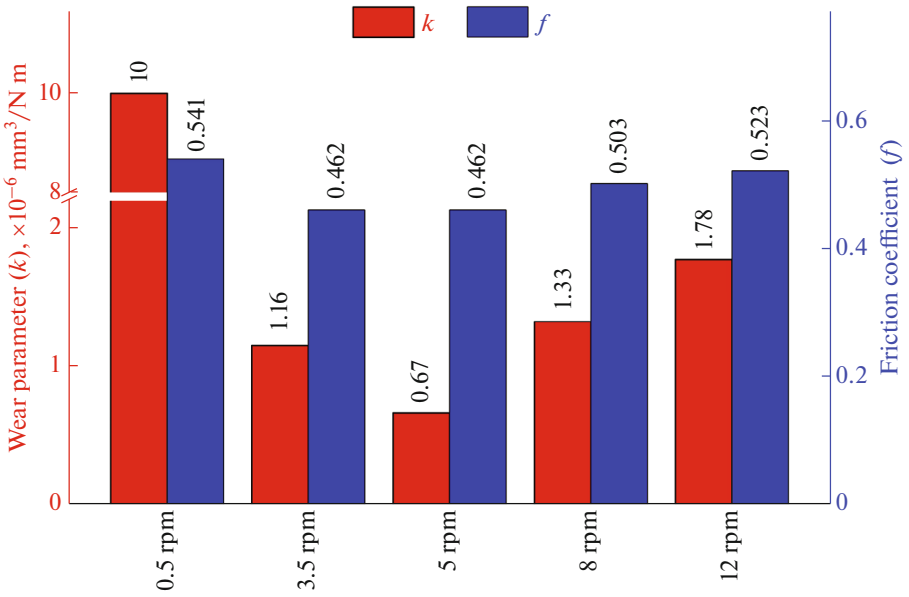

Fig. 5. Wear parameter and friction coefficient of the studied CrN/AlN coatings.

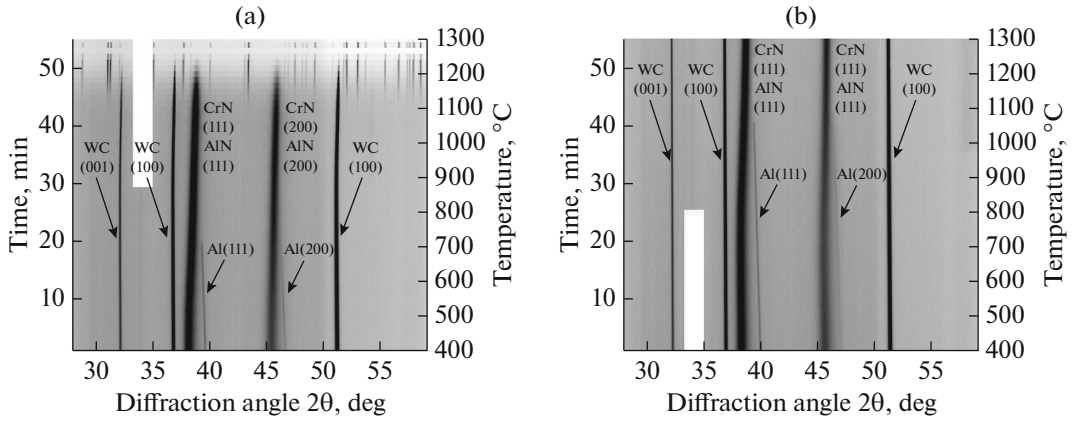

Fig. 6. Complete set of diffraction patterns of CrN/AlN 12-rpm coatings during heating from room temperature to 1300°C (a) in air and (b) in a vacuum chamber with a residual pressure of $P = 5 \times 10^{-3}$ mbar in the representation of projection of the intensity onto the "diffraction angle–temperature" plane. The white stripe is a defect in the sensor element of the detector, which does not always manifest itself in operation, and does not affect the other sensitive elements.

obtained at 12 rpm consists of chromium and aluminum nitrides, the reflections of which belong to a cubic lattice, which is a superposition of two phases. The reflections of metallic aluminum in an amount of ~5–12% are also present in the diffraction patterns. During heating, a change in the unit-cell parameters of chromium and aluminum nitrides, as well as of metallic aluminum, is observed indicating the mutual dissolution of the components. This process continues up to a temperature of ~725–730°C in air (Fig. 6a) and up to ~1050–1060°C in vacuum (Fig. 6b), after which the reflections of aluminum disappear, and the reflections of chromium and aluminum nitrides show only a shift because of thermal expansion. Chromium and aluminum nitrides retain the thermal stability (heating in air, Fig. 6a) up to a temperature of ~1110–1115°C, after which oxidation of the CrN/AlN coating begins; the reflections of chromium and aluminum nitrides disappear at a temperature of ~1235–1240°C. When heated in vacuum, chromium and aluminum nitrides retain their thermal stability at least up to a temperature of 1300°C (Fig. 6b).

CONCLUSIONS

In the course of the studies, it was found that CrN/AlN coatings have almost the same elemental composition. According to the results of X-ray phase analysis, it was found that CrN/AlN coatings have a two-phase structure consisting of CrN and AlN phases with a face-centered cubic lattice. It was established that the CSR size in the CrN/AlN coatings varies within the range from 29 to 44 nm for CrN and from 16 to 38 nm for AlN. It was established that during the process of coating sputtering, microstresses in AlN layers tend to decrease, and in CrN layers they tend to increase with increasing rotation speed. Nanoindentation revealed that the nanohardness values of the coatings vary from 28 to 33 GPa within the confidence interval, i.e., they are practically independent of the sputtering modes. The best tribotechnical characteristics were exhibited by the CrN/AlN coating obtained at a rotation speed of 5 rpm; probably under this deposition condition the optimal thickness of the CrN and AlN layers is formed. Using X-ray phase analysis with synchrotron radiation, it was established that chromium and aluminum nitrides retain thermal stability to a temperature of ~1110–1115°C when heated in air, and at least to a temperature of 1300°C when heated in vacuum.

FUNDING

The study was carried out with financial support of the Russian Federation represented by the Ministry of Science and Higher Education (project no. 075-15-2021-1348) as part of activity no. 2.1.15.

CONFLICT OF INTEREST

The authors of this work declare that they have no conflicts of interest.

REFERENCES

1. D. C. Kothari and A. N. Kale, Surf. Coat. Technol. **158–159**, 174 (2002). https://doi.org/10.1016/S0257-8972(02)00198-6
2. W. Kalss, A. Reiter, V. Derflinger, C. Gey, and J. L. Endrino, Int. J. Refract. Met. Hard Mater. **24**, 399 (2006). https://doi.org/10.1016/j.ijrmhm.2005.11.005
3. A. V. Kolubaev, O. V. Sizova, Yu. A. Denisova, A. A. Leonov, N. V. Teryukalova, and A. V. Belyi, Obrab. Met. (Tekhnol., Oborud., Instrum.) **22** (4), 137 (2020). https://doi.org/10.17212/1994-6309-2020-22.4-137-150
4. A. D. Korotaev, A. N. Tyumentsev, Yu. P. Pinzhin, Koval' N.N., I. M. Goncharenko, A. A. Tukhfatullin, V. A. Nesterenko, and V. Yu. Moshkov, Poverkhn.: Rentgenovskie, Sinkhrotronnye Neitr. Issled., No. 12, 15 (2004).
5. A. D. Pogrebnyak and Yu. A. Kravchenko, Poverkhn.: Rentgenovskie, Sinkhrotronnye Neitr. Issled., No. 11, 74 (2006).
6. T. A. Kuznetsova, V. A. Lapitskaya, S. A. Chizhik, Varkholinskii B., Gilevich A., S. M. Aizikovich, B. I. Mitrin, and L. I. Krenev, J. Surf. Invest.: X-ray, Synchrotron Neutron Tech. **14**, 1032 (2020). https://doi.org/10.1134/S1027451020050328
7. G. S. Fox-Rabinovich, G. C. Weatherly, A. I. Dodonov, A. I. Kovalev, L. S. Shuster, S. C. Veldhuis, G. K. Dosbaeva, D. L. Wainstein, and M. S. Migranov, Surf. Coat. Technol. **177–178**, 800 (2004). https://doi.org/10.1016/j.surfcoat.2003.05.004
8. G. S. Fox-Rabinovich, B. D. Beake, J. L. Endrino, S. C. Veldhuis, R. Parkinson, L. S. Shuster, and M. S. Migranov, Surf. Coat. Technol. **200**, 5738 (2006). https://doi.org/10.1016/j.surfcoat.2005.08.132
9. Y. P. Feng, L. Zhang, R. X. Ke, Q. L. Wan, Z. Wang, and Z. H. Lu, Int. J. Refract. Met. Hard Mater. **43**, 241 (2013). https://doi.org/10.1016/j.ijrmhm.2013.11.018
10. R. E. Galindo, J. L. Endrino, R. Martinez, and J. M. Albella, Spectrochim. Acta, Part B **65**, 950 (2010). https://doi.org/10.1016/j.sab.2010.09.005
11. A. D. Teresov, Yu. A. Denisova, V. V. Denisov, A. A. Leonov, E. A. Petrikova, and S. S. Koval'skii, Russ. Phys. J. **64**, 2162 (2021). https://doi.org/10.1007/s11182-022-02569-6
12. M. Schlogl, B. Mayer, J. Paulitsch, and P. H. Mayrhofer, Thin Solid Films. **545**, 375 (2013). https://doi.org/10.1016/j.tsf.2013.07.026
13. A. V. Filippov, N. N. Shamarin, E. N. Moskvichev, O. S. Novitskaya, E. O. Knyazhev, Yu. A. Denisova, A. A. Leonov, and V. V. Denisov, Obrab. Met. (Tekhnol., Oborud., Instrum.) **24** (1), 87 (2022). https://doi.org/10.17212/1994-6309-2022-24.1-87-102

14. A. V. Kolubaev, O. V. Sizova, Yu. A. Denisova, A. A. Leonov, N. V. Teryukalova, O. S. Novitskaya, and A. V. Belyi, Phys. Mesomech. **25**, 306 (2022). https://doi.org/10.1134/S102995992204004X

15. X. Chu and S. A. Barnett, J. Appl. Phys. **77**, 4403 (1995). https://doi.org/10.1063/1.359467

16. M. Kato, T. Mori, and L. H. Schwartz, Acta Metall. **28**, 285 (1980). https://doi.org/10.1016/0001-6160(80)90163-7

17. J. S. Koehler, Phys. Rev. B **2**, 547 (1970). https://doi.org/10.1103/PhysRevB.2.547

18. S. L. Lehoczky, J. Appl. Phys. **49**, 5479 (1978). https://doi.org/10.1063/1.324518

19. C. Ducros and F. Sanchette, Surf. Coat. Technol. **201**, 1045 (2006). https://doi.org/10.1016/j.surfcoat.2006.01.029

20. M. Tomlinson, S. B. Lyon, P. Eh. Hovsepian, and W. D. Munz, Vacuum **53**, 117 (1999). https://doi.org/10.1016/S0042-207X(98)00405-9

21. P. Eh. Hovsepian and W. D. Munz, Vacuum **69**, 27 (2003). https://doi.org/10.1016/S0042-207X(02)00305-6

22. P. Eh. Hovsepian, D. B. Lewis, Q. Luo, W. D. Munz, P. H. Mayrhofer, C. Mitterer, Z. Zhou, and W. M. Rainforth, Thin Solid Films **485**, 160 (2005). https://doi.org/10.1016/j.tsf.2005.03.048

23. G. S. Kim, S. Y. Lee, J. H. Hahn, and S. Y. Lee, Surf. Coat. Technol. **171**, 91 (2003). https://doi.org/10.1016/S0257-8972(03)00244-5

24. J. Lin, J. J. Moore, B. Mishra, M. Pinkas, X. Zhang, and W. D. Sproul, Thin Solid Films **517**, 5798 (2009). https://doi.org/10.1016/j.tsf.2009.02.136

25. J. K. Park and Y. J. Baik, Surf. Coat. Technol. **200**, 1519 (2005). https://doi.org/10.1016/j.surfcoat.2005.08.099

26. R. Mundotia, T. Ghorude, D. C. Kothari, A. Kale, and N. Thorat, Appl. Surf. Sci. Adv. **7**, 100205 (2022). https://doi.org/10.1016/j.apsadv.2021.100205

27. S. K. Tien, J. G. Duh, and J. W. Lee, Surf. Coat. Technol. **201**, 5138 (2007). https://doi.org/10.1016/j.surfcoat.2006.07.094

28. K. Bobzin, T. Brogelmann, R. H. Brugnara, and N. C. Kruppe, Surf. Coat. Technol. **284**, 222 (2015). https://doi.org/10.1016/j.surfcoat.2015.07.074

29. J. Vetter, E. Lugscheider, and S. S. Guerreiro, Surf. Coat. Technol. **98**, 1233 (1998). https://doi.org/10.1016/S0257-8972(97)00238-7

30. E. Mohammadpour, Z. -T. Jiang, M. Altarawneh, Z. Xie, Z. F. Zhou, Mondinos N., J. Kimpton, and B. Z. Dlugogorski, Thin Solid Films **599**, 98 (2016). https://doi.org/10.1016/j.tsf.2015.12.055

31. V. V. Denisov, Yu. A. Denisova, E. L. Vardanyan, E. V. Ostroverkhov, A. A. Leonov, and M. V. Savchuk, Russ. Phys. J. **64**, 145 (2022). https://doi.org/10.1007/s11182-021-02310-9

32. V. M. Savostikov, Yu. A. Denisova, V. V. Denisov, A. A. Leonov, S. V. Ovchinnikov, and M. V. Savchuk, Russ. Phys. J. **64**, 2219 (2022). https://doi.org/10.1007/s11182-022-02580-x

33. A. A. Leonov, E. V. Abdul'menova, M. P. Kalashnikov, and Ts. Li, Vopr. Materialoved., No. 4, **132** (2020). https://doi.org/10.22349/1994-6716-2020-104-4-132-143

34. A. A. Leonov, E. V. Abdulmenova, and M. P. Kalashnikov, Inorg. Mater.: Appl. Res. **12**, 482 (2021). https://doi.org/10.1134/S2075113321020313

35. A. A. Leonov, E. V. Abdul'menova, M. A. Rudmin, and Ts. Li, Pis'ma Mater. **11**, 452 (2021). https://doi.org/10.22226/2410-3535-2021-4-452-456

36. A. A. Leonov, E. S. Dvilis, O. L. Khasanov, V. D. Paygin, M. P. Kalashnikov, M. S. Petukevich, and A. A. Panina, Nanotechnol. Russ. **14**, 118 (2019). https://doi.org/10.1134/S1995078019020095

37. M. Falsafein, F. Ashrafizadeh, and A. Kheirandish, Surf. Interfaces. **13**, 178 (2018). https://doi.org/10.1016/j.surfin.2018.09.009

38. J. R. Tuck, A. M. Korsunsky, D. G. Bhat, and S. J. Bull, Surf. Coat. Technol. **139**, 63 (2001). https://doi.org/10.1016/S0257-8972(00)01116-6

39. D. D. Kumar, N. Kumar, S. Kalaiselvam, S. Dash, and R. Jayavel, Surfaces and Interfaces. **7**, 74 (2017). https://doi.org/10.1016/j.surfin.2017.03.001

40. H. C. Barshilia and K. S. Rajam, Bull. Mater. Sci. **26**, 233 (2003). https://doi.org/10.1007/BF02707797

41. J. Lin, J. J. Moore, B. Mishra, M. Pinkas, and W. D. Sproul, Surf. Coat. Technol. **204**, 936 (2009). https://doi.org/10.1016/j.surfcoat.2009.04.013

42. J. Lin, B. Mishra, J. J. Moore, and and W. D. Sproul, Surf. Coat. Technol. **201**, 4329 (2006). https://doi.org/10.1016/j.surfcoat.2006.08.090

Translated by S. Rostovtseva